

Correlated Eigenvalues Optical Communications

Wen Qi Zhang^{*1}, Tao Gui^{*2}, Qun Zhang³, Chao Lu⁴, Tanya M. Monro^{1,5}, Terence H. Chan³, Alan Pak Tao Lau², and Shahraam Afshar V.^{1,5}

¹Laser Physics and Photonic Devices Laboratories, School of Engineering, University of South Australia, Australia

²Department of Electrical Engineering, Photonics Research Center, The Hong Kong Polytechnic University

³Institute for Telecommunications Research, University of South Australia, Australia

⁴Department of Electronic and Information Engineering, Photonics Research Center, The Hong Kong Polytechnic University

⁵Institute for Photonics and Advanced Sensing, School of Physical Sciences, The University of Adelaide, Australia

Abstract—There is a fundamental limit on the capacity of fibre optical communication system (Shannon Limit). This limit can be potentially overcome via using Nonlinear Frequency Division Multiplexing. Dealing with noises in these systems is one of the most critical parts in implementing a practical system.

In this paper, we discover and characterize the correlations among the NFT channels. It is demonstrated that the correlation is universal (i.e., independent of types of system noises) and can be exploited to maximize transmission throughput. We propose and experimentally confirm a noise model showing that end-to-end noise can be modeled as the accumulation of noise associated with each segment of optical communication which can be dealt with independently. Also, each point noise can be further decomposed into different components, some of which are more significant (and even dominating) than others. Hence, one can further approximate and simplify the noise model by focusing on the significant component.

I. INTRODUCTION

Data traffic has been growing at a rate of more than 60% per year [1]. Such astronomical growth has sparked an urgent need to significantly increase the network transmission capacity, posing a critical technical challenge for system designers. One main fundamental challenge to further enhance data transmission bandwidth is to manage fibre nonlinearities [2].

Signal propagation across an optical fibre is governed by the nonlinear Schrödinger equation. The channel is nonlinear, unlike other typical transmission media such as copper wires and radio waves [2]. Traditionally, fibre nonlinearities are often regarded as channel impairments, and hence should be eliminated or mitigated. Instead of dealing with fibre nonlinearities directly, existing schemes are often based on a “flawed” approach in that they apply “off-the-shelf” methods originally developed for classical linear time-invariant radio frequency channels (typically with additive white Gaussian noise). This approach ignores the detail of the underlying fibre physics, and attempts to draw loose analogies between macroscopic channel impairments (e.g. dispersion caused by a linear multipath channel) encountered in microwave channels with those in optical channels (e.g. dispersion due to wavelength-dependent refractive index, fibre geometry or nonlinearities). In essence,

nonlinearities are assumed to be weak and hence can be treated and suppressed as small perturbations [3], [4].

The underlying premise behind this perspective is that signals are processed often in the time domain and/or the (linear) frequency domain (where signals are obtained by applying linear transformation such as Fourier transform on the time-domain signals). However, fibre nonlinearities cannot be completely eliminated by invoking these linear signal processing techniques, leading to undesirable inter-symbol interference (ISI) and inter-channel interference (ICI) [4]. As a result, it was noted that fibre nonlinearities can impose a fundamental limit (known as linear Shannon limit) on the data transmission capacity [3].

A different paradigm to the problem has received a lot of attentions in the past few years. In this paradigm, fibre nonlinearity and dispersion effect are merely seen as ordinary physical characteristics needed to be managed directly, rather than simply evading them as disadvantages [5]–[8]. In particular, their approaches are based on the use of nonlinear Fourier transform (NFT), or direct scattering transform [9]–[11]. Higher order dispersion effects are often ignored, and the linear loss term is assumed to be perfectly compensated by the distributed Raman amplification (DRA).

Mathematically, the NFT provides a systematic method for solving the class of integrable nonlinear Schrödinger equation, whereas in engineering perspective, NFT can “decompose” the nonlinear fibre channel into multiple independent subchannels in the (nonlinear) spectral domain. To a great extent, it mirrors the widely used wavelength-division multiplexing (WDM), a technology which multiplexes multiple optical carrier signals and transmitted in a single optical fibre. The fundamental difference between WDM and NFT based approach is in how the “modes” or “subchannels” are defined.

Roughly speaking, WDM employs Fourier Transform (FT) such that each wavelength (or its corresponding linear frequency) is essentially a “transmission mode”. When signal-to-noise ratio (SNR) is low and nonlinearities are not severe, interference among these modes are negligible. However, as data rate (and also signal power) increases, nonlinearities become significant and the transmission modes defined by FT can now significantly interfere with each other. This significantly limits the performance of the fibre-optic communications systems,

*These authors have contributed similarly to the paper

especially in long-haul transmissions. In [6], NFT was used instead of FT, such that the resulting nonlinear normal modes will not interfere with each other even in the presence of nonlinear effects. This idea of decoupling a nonlinear channel into multiple independent subchannels plays the central role in NFT based communications. As a result of the channel decomposition, one can separately design communications for each individual subchannel, and hence greatly reduce the system complexity. Also, inter-channel interference is eliminated with a proper allocation of the (nonlinear) spectrum to users at least in the noise free scenario. This scheme is called nonlinear frequency division multiplexing (NFDM) [6].

The development of NFT-based transmission systems is only in its infancy stage at the moment. Some preliminary experimental works have already been done to demonstrate the concepts. The spectrum of a time domain signal, after applying the NFT, is composed by discrete and continuous spectrum. Both continuous [6], [12]–[15] and discrete [16]–[21] spectra have been proposed for optical transmission systems. Using a discrete 1-, 2-, 3-eigenvalue configuration together with on-off keying, Dong *et. al.*, [16] have achieved 1.5 Gbps transmission over 1800 km. In [22] a two-eigenvalue signal together with QPSK modulation has been used to achieve 4 Gbps transmission rate over 640km. Optical transmission using continuous spectrum, has recently been demonstrated by Le *et. al* [14], where a 120 bits/burst transmission over 7344 km has been achieved.

As mentioned above, NFT based methods lead to channel decomposition with zero inter-channel interference. Unfortunately, perfect channel decomposition is only theoretically possible in the absence of noise. In practice, noise can be generated in the transmitter and the receiver (e.g., quantization, clipping), and also during propagation in the fiber (e.g., due to inline or point amplification). These noises will induce correlations among individual subchannels, affecting the capacity of the transmission system. Despite the crucial role of noise in determining the actual capacity of an NFT-based transmission system, effects of noise on NFT continuous and discrete spectra have only been studied in limited cases. Zhang *et. al.* [23], have studied the effect of propagation noise (with Gaussian distribution) on the spectral amplitudes and the discrete eigenvalue of the channel output when the input is a fundamental soliton. In addition, Derevyanko *et. al.*, [24] have developed an approximated noise (with Gaussian distribution) model for continuum spectra NFT based transmission and estimated a lower bound for the capacity. Based on their model, they find the noise properties of NFT continuous spectra after propagating through a fiber in presence of noise.

In this paper, we investigate the noise properties of optical communications systems based on input optical pulses with discrete NFT eigenvalues. There are four main aspects in our contributions. *First*, we demonstrate that the discrete eigenvalues of a signal propagating through the network are correlated, regardless of the different types of noise that have been introduced at different stages of signal preparation, propagation, and detection. We show that such correlation properties can be used to maximize the transmission throughput so that input signal constellation can be optimized to support high data

transmission rate.

Second, we propose and experimentally confirm a noise model, in which deterministic (due to nonlinearity and dispersion) and stochastic (due to all noises) effects on signals can be separately evaluated in a similar fashion as linear and nonlinear processes in Split Step Method.

Third, it is shown that the noise effects do not accumulate and noise associated with each segment of optical communication can be dealt independently.

Finally, as a result of second and third properties, we identify and demonstrate that the effect of noise can be decomposed into different components and some noise components are more significant than others. This suggests that one can further approximate and simplify noise effects by focusing on those significant noise components.

II. BASIC PRINCIPLE

The noisy signal evolution across an optical fibre is often modelled as the following stochastic nonlinear Schrödinger equation (SNLSE)

$$\begin{aligned} \frac{\partial A(s, l)}{\partial l} - \frac{j\beta_2}{2} \frac{\partial^2 A(s, l)}{\partial s^2} + \frac{\alpha}{2} A(s, l) = \\ - j\gamma |A(s, l)|^2 A(s, l) + j\kappa N(s, l), \end{aligned} \quad 0 \leq l \leq \mathfrak{L} \text{ km}, \quad (1)$$

where $j = \sqrt{-1}$. The function $A(s, l)$ is the complex envelope of the signal propagating along the fibre. The parameter β_2 is the group velocity dispersion (GVD) coefficient. The GVD coefficient for silica fibres is $\beta_2 = -2 \times 10^{-23} \text{ s}^2 \cdot \text{km}^{-1}$ when the input wavelength is $1.55 \mu\text{m}$. The parameter α is called attenuation coefficient which describes the (linear) loss effect, and γ is the nonlinear coefficient. The positive real number \mathfrak{L} denotes the length of the optical fiber. The term $j\kappa N(\tau, l)$ represents the optical noise field, which could be modelled as a zero mean circularly symmetric complex white Gaussian noise process [25], [26] with

$$E[N(s, l)N^*(s', l')] = \delta(s - s')\delta(l - l'), \quad (2)$$

where we use “*” to denote the complex conjugate, and $\delta(x)$ means Dirac delta function, and κ is a coefficient that determines the strength of the noise. After applying the following variable transformations

$$q = \frac{A}{\sqrt{P}}, \quad t = \frac{s}{T}, \quad z = \frac{l}{\mathfrak{L}}, \quad (3)$$

where

$$P = \frac{2}{\gamma \mathfrak{L}}, \quad T = \sqrt{\frac{|\beta_2| \mathfrak{L}}{2}}, \quad (4)$$

we obtain the normalised SNLSE

$$jq_z(t, z) = q_{tt}(t, z) + 2|q(t, z)|^2 q(t, z) + j\epsilon G(t, z), \quad (5)$$

where the noise $\epsilon G(t, z)$ is a zero mean circularly symmetric complex white Gaussian noise with power spectral density $\epsilon^2 = \frac{\gamma}{\sqrt{2}|\beta_2|} \kappa^2$. Under the model (5), the effect of noise in soliton parameters was studied. In particular, the statistics of the eigenvalue was reported in [27], [28], and the arrival

time jitter, namely Gordon-Haus effect, was studied in the celebrated paper [29]. The research about soliton transmission control, regarding the issue of timing jitter, can be found in [30]–[33]. The Gordon-Mollenauer effect, referring to the soliton phase jitter, was investigated in [34], and the work about its statistics in solitonic dispersion phase shift keying systems was studied in [35]–[38].

Let L be an operator on $q(t, z)$ where

$$L = j \begin{pmatrix} \frac{\partial}{\partial t} & -q(t, z) \\ -q^*(t, z) & -\frac{\partial}{\partial t} \end{pmatrix}, \quad (6)$$

The eigenvalues of the operator L are invariant in z as the signal $q(t, z)$ propagates through the fibre. In the definition of the NFT, we suppress the variable z because it is only useful when we need to derive the spatial signal propagation through an optical fibre. Throughout this paper, we assume that $q(t) \in L^1(\mathbb{R})$ and $q(t) \rightarrow 0$, $t \rightarrow \infty$.

The NFT of a signal $q(t)$ is defined via the spectral analysis of the operator L . Specifically, we need to solve the eigenvalue problem

$$Lv = \lambda v$$

at first, which is equivalent to the ordinary differential equation (ODE)

$$v_t = \begin{pmatrix} -j\lambda & q(t) \\ -q^*(t) & j\lambda \end{pmatrix} v \quad (7)$$

called the scattering problem. Using boundary conditions

$$\lim_{t \rightarrow -\infty} \left| v(t, \lambda) - \begin{pmatrix} 1 \\ 0 \end{pmatrix} e^{-j\lambda t} \right| = 0, \quad (8)$$

we obtain a solution of (7).

Let $v(t, \lambda) = [v_1(t, \lambda), v_2(t, \lambda)]^T$. The coefficients $a(\lambda)$ and $b(\lambda)$ are called scattering data, which can be obtained by calculating

$$a(\lambda) = \lim_{t \rightarrow \infty} v_1(t, \lambda) e^{j\lambda t}, \quad (9)$$

and

$$b(\lambda) = \lim_{t \rightarrow \infty} v_2(t, \lambda) e^{-j\lambda t}. \quad (10)$$

The nonlinear Fourier transform of a function $q(t)$ is defined with the help of the scattering data. The NFT of a signal $q(t)$ is composed of its spectrum and the corresponding spectral amplitudes. The spectrum is composed of the discrete and continuous spectrum. The discrete spectrum is a set of isolated complex points called (discrete) eigenvalues, which are zeros of the scattering data $a(\lambda)$ on the upper half complex plane $\mathbb{C}^+ \triangleq \{c \in \mathbb{C} : \text{Im}(c) > 0\}$. The continuous spectrum is the real line \mathbb{R} . The corresponding spectral amplitudes are defined as follows. The discrete spectral amplitude subject to an eigenvalue $\lambda_k \in \mathbb{C}^+$ is

$$Q^{(d)}(\lambda_k) = \frac{b(\lambda_k)}{a'(\lambda_k)}, \quad k = 1, 2, \dots, N, \quad (11)$$

where $a'(\lambda_k) \triangleq \left. \frac{da(\lambda)}{d\lambda} \right|_{\lambda=\lambda_k}$, and N is the number of the zeros of $a(\lambda)$. The continuous spectral amplitude is defined as

$$Q^{(c)}(\lambda) = \frac{b(\lambda)}{a(\lambda)}, \quad (12)$$

where $\lambda \in \mathbb{R}$.

It is well known that the spectrum of the signal keeps invariant as a signal propagates through an optical fibre in the noise free case. The spatial evolution of the spectral amplitudes are summarised as follows:

$$Q^{(c)}(\lambda, z) = Q^{(c)}(\lambda, 0) e^{-4j\lambda^2 z}, \quad (13)$$

and

$$Q^{(d)}(\lambda_k, z) = Q^{(d)}(\lambda_k, 0) e^{-4j\lambda_k^2 z}, \quad k = 1, 2, \dots, N, \quad (14)$$

where $Q^{(c)}(\lambda, z)$ and $Q^{(d)}(\lambda_k, z)$ are respectively a continuous and a discrete spectral amplitude at position z , and $z > 0$, and $-4j\lambda_k$ is the NFT channel gain coefficient and $e^{-4j\lambda_k^2 z}$ as the channel gain.

III. Results: EIGENVALUE CORRELATION

Pulse propagation experiments and simulations were carried out using pulses with only two discrete eigenvalues ranging from $\lambda_1 = 0.3j$ to $0.75j$ and $\lambda_2 = 0.9j$ to $1.35j$ in steps of $0.15j$.

Fig. 1 shows the experimental setup for the eigenvalue correlation transmission system. The transmitter (TX) comprises a 92-GSa/s arbitrary waveform generator (AWG) providing a drive signal for an IQ modulator which generates 1-GBd optical soliton pulses train in a single polarization. The outputs of the modulator are amplified and launched into a fiber recirculating loop. Since the theory of NFT is based on the integrability property of the lossless nonlinear Schrödinger equation, a short span of 50km NZ-DSF fiber (with $\alpha = 0.19$ dB/km, $\beta_2 = 5.01$ ps²km⁻¹ and $\gamma = 1.2$ W⁻¹km⁻¹) has been considered in the recirculating loop to best approximate constant signal power evolution along the link. An EDFA is placed after the fiber to compensate the span loss and ensure the same launched power after each loop. A flat-top optical filter with a 3db bandwidth of 1nm is used inside the loop to suppress the out-of-band (amplified spontaneous emission) ASE noise. At the receiver, the signal is first aligned in a particular polarization by a polarization controller and then detected by an integrated coherent receiver. The output electrical waveforms are sampled by a digital storage scope (with a sampling rate of 80 GSa/s and a bandwidth of 33GHz) followed by off-line digital signal processing (DSP).

Figure 2 shows the experimental and simulated received signal distributions of the group of 2-soliton pulses after propagating a distance of 400km, equivalent of 8 times circulation within the fiber loop. For each pulse set (λ_1, λ_2) simulations were ran for 500 times, with noiseless input pulses but distributed random noise within the fiber. After propagation, the eigenvalues of these 500 outputs were then calculated using a forward difference method [6], see Simulation section in Methods V-A. Figs 2a and 2b show the experimental and simulation distribution of each set of eigenvalues after propagation, respectively. A circular distribution of the two eigenvalues are expected for totally uncorrelated eigenvalues, however, the results show a linear-like distribution, which indicates a positive correlation. To quantify this we have

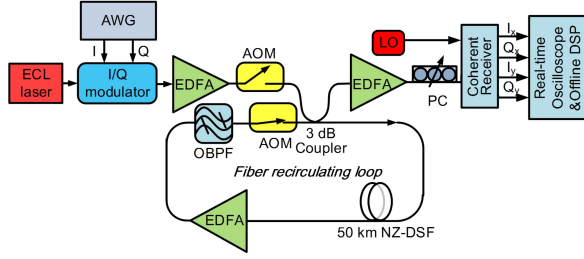


Fig. 1: Experimental setup. ECL: external cavity laser; AWG: arbitrary waveform generator; AOM: acousto-optic modulator; EDFA: erbium doped fiber amplifier; NZ-DSF: non zero dispersion shifted fiber; OBPF: Optical band pass filter; LO: local oscillator; PC: polarization controller.

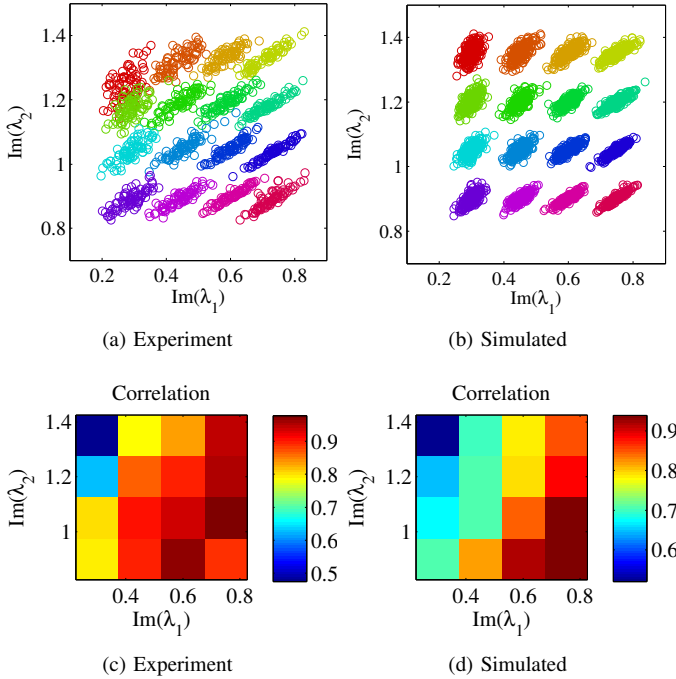


Fig. 2: Experimental, (2a), and simulated, (2b), distribution of eigenvalues after 400 km transmission. 2c and 2d, experimental and simulated contour plot of correlation parameter, respectively.

calculated the sample correlation coefficient¹ between $Im(\lambda_1)$ and $Im(\lambda_2)$ for each set of eigenvalues and represent them in Figs. 2c and d, for experimental and simulation results, respectively.

Both experimental and simulation results show the following common characteristics that indicate the correlated nature of NFT eigenvalues:

- (1) Both experiment and simulation show positive correla-

¹ The sample correlation between n samples of (x_i, y_i) for $i = 1, \dots, n$ is defined as

$$\frac{\sum_{i=1}^n (x_i - \bar{x})(y_i - \bar{y})}{(n-1)s_x s_y}$$

where 1) \bar{x} , \bar{y} are sample means of x and y , and 2) s_x and s_y are the sample standard deviations of x and y .

tion represented by elongated elliptical shapes with a slightly different orientation of major axis. From a signal design point of view, and as we demonstrate through a simulation below, one can appropriately leverage such correlation properties by more compact arranging of NFT eigenvalues in the direction of the minor axis of the elliptical distribution and achieve a higher spectral efficiency.

- (2) In both cases, correlation decreases as λ_2 increases or λ_1 decreases.

However, some discrepancies between experimental and simulation results are also observed. Qualitatively, the orientation of the distributions of the two eigenvalues and their correlation are different for experiment and simulation results, see Fig. 12 (in supplementary materials). This could be explained by noting that in simulations, we only consider white Gaussian noise added during the propagation along the fiber. In the experiment, however, apart from the noise generated during propagation, noises are also induced during the pulse generation stage (e.g., when using the AWG to generate the electrical signals and the IQ modulator to generate optical signals.) and detection stages. In general, different types of noise can affect a signal at different stages of generation, propagation, and detection. In the supplementary materials, we have investigated collectively the effects of different types of noise on the correlation eigenvalue distribution.

Correlations of NFT eigenvalues has a significant impact on designing an NFT-based fiber optic network. In the following, we consider an example illustrating how to exploit such correlations to improve the performance of a system.

Example: Consider input signal constellation of 2-solitons pulses, with eigenvalues $\lambda_1 \in [0.7j, 0.74j, 0.78j, 0.82j]$ and $\lambda_2 \in [0.9j, 0.92j, \dots, 1.00j, 1.02j]$. For each input, we propagate the signal in a fibre for a normalised distance of 0.1. Figure 3(a), shows the distribution of the two eigenvalues for the output pulses, clearly showing correlation between the eigenvalues. Now, suppose the correlation is ignored. Then the decoder will assume in the worst case that the two eigenvalues are independently distributed. Figure 3(b) shows the distribution of two eigenvalues assuming that they are in fact independently distributed. This leads to the requirement that the eigenvalues of input signals should be separated sufficiently enough to ensure that the decoder can distinguish different inputs with high accuracy. On the other hand, by exploiting correlations, we can pack more inputs with eigenvalues in range of $[0.7j, 0.82j]$ and $[0.9j, 1.02j]$ such that the decoder can still decode with low error probability. Figure, 3(c) shows a 10 fold larger constellation, using the same range of eigenvalues for λ_1 and λ_2 , but denser packing of the eigenvalues of input signals. In this example, the data rate has been increased from $\log 24$ bits per symbol to $\log 84$ bits per symbol, equivalent to approximately 39 percent increase in data rate. Clearly, the actual increase in data rate will depend on a lot of other factors, such as power and bandwidth constraint.

Remark: The above example is used only to demonstrate how correlations can be exploited to increase data rate.

Further simulation studies reveals that the correlation exists

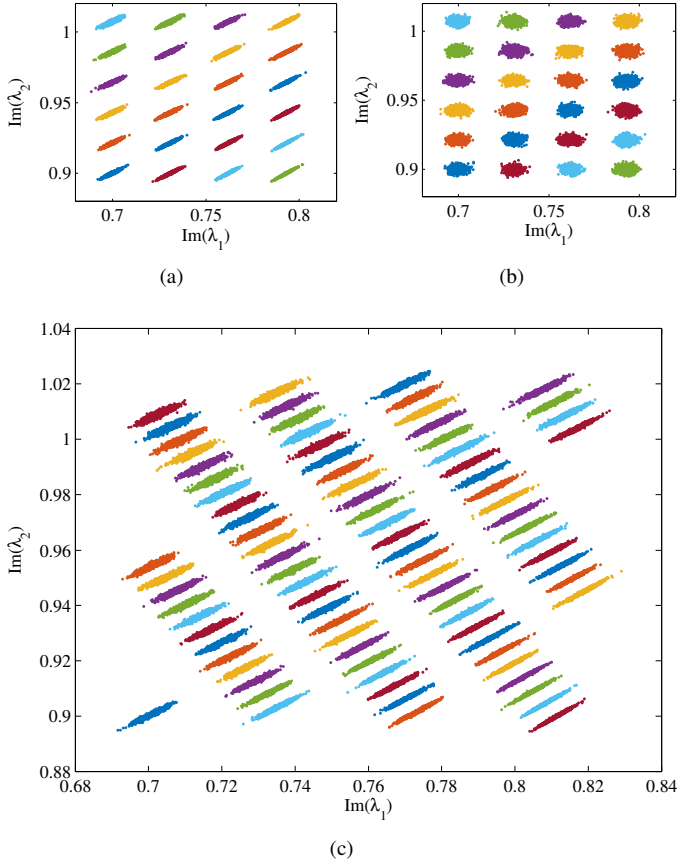


Fig. 3: Distribution of eigenvalues for constellation of 2-soliton pulses after propagating for 0.1 normalized distance. (a) distribution of eigenvalues for a $4 \times 6 = 24$ constellation. (b) distribution of eigenvalues for a 4×6 constellation but assuming no correlation. (c) distribution of eigenvalues for a 83 constellation.

in systems with larger number of discrete eigenvalues, e.g. 3. Figure 4 shows a case with 3 discrete eigenvalues $0.5j$, $1.5j$ and $2.5j$. The subplots of Fig. 4 show the correlation between eigenvalues λ_1 and λ_2 , λ_1 and λ_3 , λ_2 and λ_3 as well as a distribution of the eigenvalues in a 3-D parameter space. Similar correlations can also be found in systems with even more eigenvalues.

IV. Results: MODELING EIGENVALUES PERTURBATION

One fundamental challenge in designing eigenvalue communications system is to characterize the noise in the discrete eigenvalues. In the previous section, we have discussed the correlation of discrete eigenvalues for short distance (of normalized length 0.1) experimentally and numerically. In the following, we will develop a full model of eigenvalue perturbation, based on our two observations on properties of NFT discrete eigenvalue perturbation in an optical communication system:

- 1) **Split Step Method for noise;** deterministic (due to nonlinearity and dispersion) and stochastic (e.g., due to all signal amplification) noise effects can be separated,

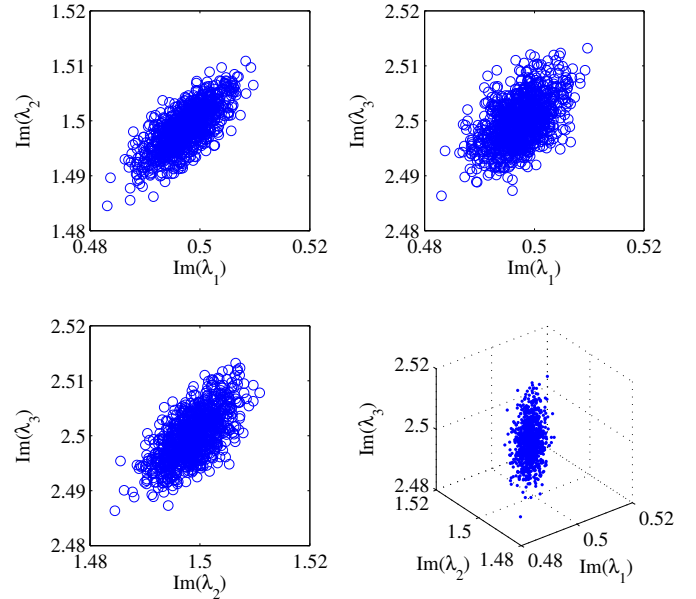


Fig. 4: (a), (b), (c) Correlations between all possible pairs of eigenvalues for a 3-eigenvalue input signal. (d) correlation of all eigenvalues in 3 dimensional parameter space.

in a similar fashion as linear and nonlinear processes in Split Step Method, and

- 2) **No noise hysteresis;** the effect of noise associated with each segment of optical communication can be dealt independently.

First, we will state the framework based on which the eigenvalue noise perturbation model is developed. When a signal propagates along a fibre, it will be distorted by various channel impairments² such as noises and fibre nonlinearity and dispersion, causing its shape to change during propagation. To model the process, we treat a fibre as a concatenation of many short fibre segments. As each segment is short, fibre nonlinearity and noise can often be modeled separately. Under this model, when a signal propagates in a segment, it will undergo two phases. In the first phase, it will be distorted by fibre nonlinearity, assuming that the segment is noiseless. Then in the next phase, a white Gaussian noise (whose power is proportional to the length of the fibre segment) will be added. The resulting signal will then become the input of the next segment, and the same process will continue until it reaches the end of the fibre, see Fig. 5.

Modeling a fibre as a concatenation of short segments is only the first step. Due to fibre nonlinearities and the coupling effects between noises and signals, it is still very difficult to derive an analytic model to characterise the eigenvalues perturbations. In the following, we aim to simplify the model.

A. Simplification 1: Noise Decoupling

One of the challenges in deriving a model for characterising the perturbation of discrete eigenvalues is due to the coupling

²In this paper, we will assume that the fibre loss can be perfectly compensated by inline distributed amplification.

TABLE I: Notations

Symbol	Definition	Symbol	Definition
$q_m(t)$	output of signal after propagating m segment	Λ_m	discrete eigenvalues of $q_m(t)$
$\bar{q}_m(t)$	output of signal after propagating m segment, assuming no added stochastic noises	$\hat{\Lambda}_m$	discrete eigenvalues of $\hat{q}_m(t)$
$n_m(t)$	noises added in the m segment	$g(\Lambda)$	a function of Λ
$\hat{q}_m(t)$	$\bar{q}_m(t) + n_m(t)$		

effects of stochastic signal dependent noises (e.g., due to inline amplification) and the distortion due to nonlinearities and dispersions. In the following, we propose a new simplification paradigm to decouple the two noise effects. Our proposed simplification is based on the observation that *perturbation of eigenvalues at the end of the fibre can be accurately modelled by “summing up” all the small perturbations of eigenvalues in the segments.*

Suppose the input to the fibre is $q_0(t)$. Divide the fibre into M segments and let $q_m(t)$ be the output of the signal after propagating m segments (or equivalently the input to the $(m + 1)^{th}$ segment). Define Λ_m as the set of discrete eigenvalues of $q_m(t)$. Let $g(\Lambda_m)$ be a (scalar or vector valued) function of Λ_m of interest.

Notice that

$$g(\Lambda_M) - g(\Lambda_0) = \sum_{m=1}^M g(\Lambda_m) - g(\Lambda_{m-1}).$$

Therefore, we can characterise the perturbation $g(\Lambda_M) - g(\Lambda_0)$ by characterising the perturbation $g(\Lambda_m) - g(\Lambda_{m-1})$ for all m , see Fig. 5.

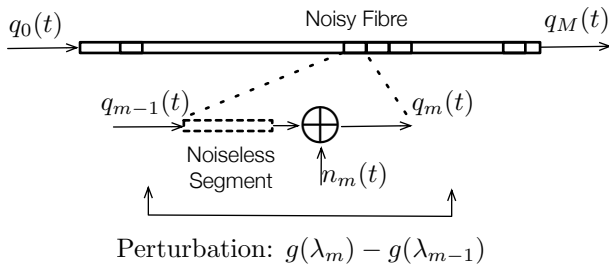


Fig. 5: Channel Model: Fiber is considered as a concatenation of M segments. The perturbation of eigenvalues (or their function values) is modeled as the accumulation of many perturbations caused by the addition of noises in each segment. Each perturbation ϵ_m is further modelled as independent, depending only on the deterministically distorted signal $\bar{q}_m(t)$.

Observing each individual term, the perturbation $g(\Lambda_m) - g(\Lambda_{m-1})$ is caused by the injection of a noise at the m^{th} segment. First, we want to point out that the perturbation depends on both the injected noise $n_m(t)$ and the input of the segment $q_{m-1}(t)$ (which in turn also depends on the noises added in the previous segments). However, we claim that; *the influence due to the noise added in the previous segments are insignificant (and hence can be ignored).*

Let $\bar{q}_m(t)$ be the output of the signal after propagating through m^{th} segments, assuming there are no noises. Hence, $\bar{q}_m(t)$ is a deterministic signal. Due to fibre nonlinearity, its shape will vary with m . However, the discrete eigenvalues for all $\bar{q}_m(t)$ remained unchanged. Let $n_m(t)$ be the noise added in the m segments,

$$\hat{q}_m(t) = \bar{q}_m(t) + n_m(t) \quad (15)$$

and $\hat{\Lambda}_m$ be its set of discrete eigenvalues. In other words, \hat{q}_m is obtained by propagating $q_0(t)$ noiselessly across m segments, followed by the addition of the noise $n_m(t)$. See Figure 5. We claim that $g(\hat{\Lambda}_m) - g(\Lambda_0)$ is in indeed a good approximation for $g(\Lambda_m) - g(\Lambda_{m-1})$. Let $\epsilon_m = g(\hat{\Lambda}_m) - g(\Lambda_0)$. Then $g(\Lambda_M) - g(\Lambda_0) \approx \sum_{m=1}^M \epsilon_m$ or equivalently,

$$g(\Lambda_M) \approx g(\Lambda_0) + \sum_{m=1}^M \epsilon_m. \quad (16)$$

Benefits: The above approximation points out that the end-to-end perturbation is now modelled as the sum of a collection of independently distributed local perturbations (as \bar{q}_m is deterministic and the noise $n_m(t)$ is independently distributed for all m). The main benefit of the model is its simplicity, decoupling the stochastic noises (caused by inline amplification) from the deterministic dispersion and nonlinearities.

To be more precise, we have already seen that the local perturbation of the eigenvalues

$$g(\hat{\Lambda}_m) - g(\Lambda_0)$$

depends on m (and more precisely the signal that enters the m fibre segment, i.e., $\bar{q}_m(t)$). This same argument also applies to the local perturbation that

$$g(\Lambda_m) - g(\Lambda_{m-1})$$

also depends on the signal $q_{m-1}(t)$ which is stochastic in nature due to the noises added in the previous $m - 1$ segments. In that case, the stochastic random noise and the deterministic dispersion and nonlinearities will couple with each other. Furthermore,

$$g(\Lambda_m) - g(\Lambda_{m-1})$$

will become correlated for different m . Our approximation decouples the two effects, resulting in a simpler mode. Through the approximation, we also break the correlation among local perturbations, making channel analysis more manageable.

B. Validation

In the following, we will validate Eq. (16) through numerical simulation and experiment. We investigate the perturbation of discrete eigenvalues of a 2-soliton input signal, $q_0(t) = 2\text{sech}(t)$, which has two discrete eigenvalues at $0.5j$ and $1.5j$. Specifically, the function $g(\cdot)$ is a vector valued function, corresponding to the imaginary parts of the two discrete eigenvalues of the signals propagating along the fibre. First, using numerical simulation (details of simulation method are given in V-A), we illustrate that the perturbation $\epsilon_m = g(\hat{\Lambda}_m) - g(\Lambda_0)$ is signal dependent (i.e., depending on $\bar{q}_m(t)$).

We plot the ensemble of two discrete eigenvalues of $\hat{\Lambda}_m$ for various m . Since the time domain signal will change its shape as it propagates, our numerical example clearly shows that not only the two eigenvalues are all correlated, but how they correlate depend on m as well (See Figure 6). This supports our observation that the statistics of $g(\hat{\Lambda}_m)$ (and hence also $g(\hat{\Lambda}_m) - g(\Lambda_0)$ as $g(\Lambda_0)$ is a constant) depends on $\bar{q}_m(t)$. It also suggests that the statistics of $g(\Lambda_m) - g(\Lambda_{m-1})$ will also depend on $q_{m-1}(t)$ which, strictly speaking, will also be influenced by the noises injected in the previous segments.

Observing the scattering plots for $\hat{\Lambda}_m$, the mean and covariance matrix of $\hat{\Lambda}_m$ depends on m (and more precisely, on $q_{m-1}(t)$). Clearly, it also depends on the noise power. In order to better understand the influence of $q_{m-1}(t)$ on $\hat{\Lambda}_m$, we will focus on the eigenvectors (in particular the principal one) of the covariance matrices.

Now, consider a 2 soliton $q_0(t) = 2\text{sech}(t)$, which has two discrete eigenvalues at $0.5j$ and $1.5j$. Then $\bar{q}_m(t)$, obtained by propagating $q_0(t)$ for m segments, are also 2-solitons, with discrete eigenvalues at $0.5j$ and $1.5j$. Let $Q_m^{(d)}(0.5j)$ and $Q_m^{(d)}(1.5j)$ be its corresponding spectral amplitudes. Then they will vary as m increases (i.e., as the signal propagates). To make it more precise, if the normalised distance of each fibre segment is Δ_L , then $q_m(t)$ is the signal after propagating $q_0(t)$ for a distance of $m\Delta_L$. If we define $\theta(m\Delta_L)$ as the ratio $Q_m^{(d)}(0.5j)/Q_m^{(d)}(1.5j)$, then

$$\theta(m\Delta_L) = e^{4m\Delta_L(\lambda_1^2 - \lambda_2^2)j}$$

where $\lambda_1 = 0.5j$ and $\lambda_2 = 1.5j$. We call $4m\Delta_L(\lambda_1^2 - \lambda_2^2)$ the *nonlinear phase difference*.

In our example, we focus on the imaginary parts of the two discrete eigenvalues. Figure 6 plots the two discrete eigenvalues, which shows that they are correlated with each other. Also, the correlation is different for different m . For each scattering plot, we can estimate the covariance matrix between the imaginary parts of the two discrete eigenvalues. We can also plot the angle of the principal eigenvector³ of the covariance matrix. It turns out that the principal eigenvector of the covariance matrix for $\hat{\Lambda}_m$ depends only on the nonlinear phase. Simulation results are shown in Figure 7, which clearly indicate that the principal eigenvector, and also the covariance matrix for $\hat{\Lambda}_m$ are different for different m . Note that in the simulation, a noise is added to $\bar{q}_m(t)$, which is a result of propagating $q_0(t)$ noiselessly for a distance of $m\Delta_L$.

To verify our observation and to support the simulation result, we also consider the following experiment. Our experiment set up is very similar to the one in Figure 1. EDFAs are used to amplify signals to combat signal loss. We consider a range of propagation distance up to 1500 km which consisting of 30 loops, where every 3 loops correspond to a 0.1 normalized length. This is to mimicking the generation of $\bar{q}_m(t)$. Figure 7 shows the experimental values for the orientation of principal eigenvector of covariance matrix (red

circles). A qualitative agreement is observed between experiment and simulation results. This supports the assumption that eigenvalue distribution depends on signal at that point.

Note that, in experiments, noises are added at the transmitter, the receiver and also during propagation. However, the propagation noises is small (compared to the other noises), since the propagation distances are all small in our experiments. In addition, the transmitter noise is the same in all the experiments. Therefore, the difference in the distribution of eigenvalues observed at the output for different propagation lengths are only due to the receiver noise (See supplementary material attached). In our experiment, the receiver noise acts as the role of the point noise injected in the simulation. Careful examination of the simulation and experiment results in Figure 7, shows a good agreement when the propagation distance is small. However, the two results start to become less agreeable for longer distances. This can also be explained by the fact that the propagation noise increases for longer propagation distances.

So far, we have demonstrated that the local perturbation caused by the injection of noise in a segment is not identically distributed and depends on pulse shape of the input at each segment. Next, we want to show that the overall perturbation $g(\Lambda_M) - g(\Lambda_0)$ can be approximated by accumulating individual smaller perturbations ϵ_m . In other words, we want to show that the approximation (16) is indeed fairly accurate.

To validate, we will consider the following numerical example. We consider the special case when $g_0(t)$ is a 2-soliton. In particular, we are interested in the imaginary parts of the two discrete eigenvalues of the input and output signals. In other words

$$g(\Lambda) = [Im(\lambda_1), Im(\lambda_2)]^T$$

where $\Lambda = (\lambda_1, \lambda_2)$. Here, we consider various choices of m (corresponding to propagation distance from 0.1 to 1). Results are shown in Figure 8.

Let $\Lambda_m \triangleq (\lambda_{m,1}, \lambda_{m,2})$ be the discrete eigenvalues of $q_m(t)$, the signal obtained by propagating the input signal across m fibre segments. The lower scatter plot (formed by the red circles) in Figure 8 is obtained by plotting $Im(\lambda_{m,1})$ against $Im(\lambda_{m,2})$ for various m . The upper scatter plot (formed by the blue circles) in Figure 8 is obtained using the approximation (16), defined as the sum of $g(\Lambda_0)$ and a set of local perturbations caused by the addition of noises added throughout each segment. Specifically, the RHS of (16) is

$$\begin{bmatrix} 0.5 + Im \left(\sum_{\ell=1}^m (\hat{\lambda}_{\ell,1} - 0.5j) \right) \\ 1.5 + Im \left(\sum_{\ell=1}^m (\hat{\lambda}_{\ell,2} - 1.5j) \right) \end{bmatrix}$$

where $\hat{\Lambda}_\ell = (\hat{\lambda}_{\ell,1}, \hat{\lambda}_{\ell,2})$ is the discrete eigenvalues of $\hat{q}_\ell(t)$ obtained by propagating the input signal $q_0(t)$ for ℓ segments followed by the addition of a local noise $n_\ell(t)$. Now, if we compare the two sets of scatter plots, we can see immediately that the two plots look extremely similar. This indicates that one can model the eigenvalues perturbation for Λ_m pretty accurately, by using our approximation.

³ The principal eigenvector of a covariance matrix is the matrix's eigenvector (often of unit length) with respect to the largest eigenvalue. In the case of a 2×2 matrix, we can further represent the vector by the angle it makes with the horizontal axis.

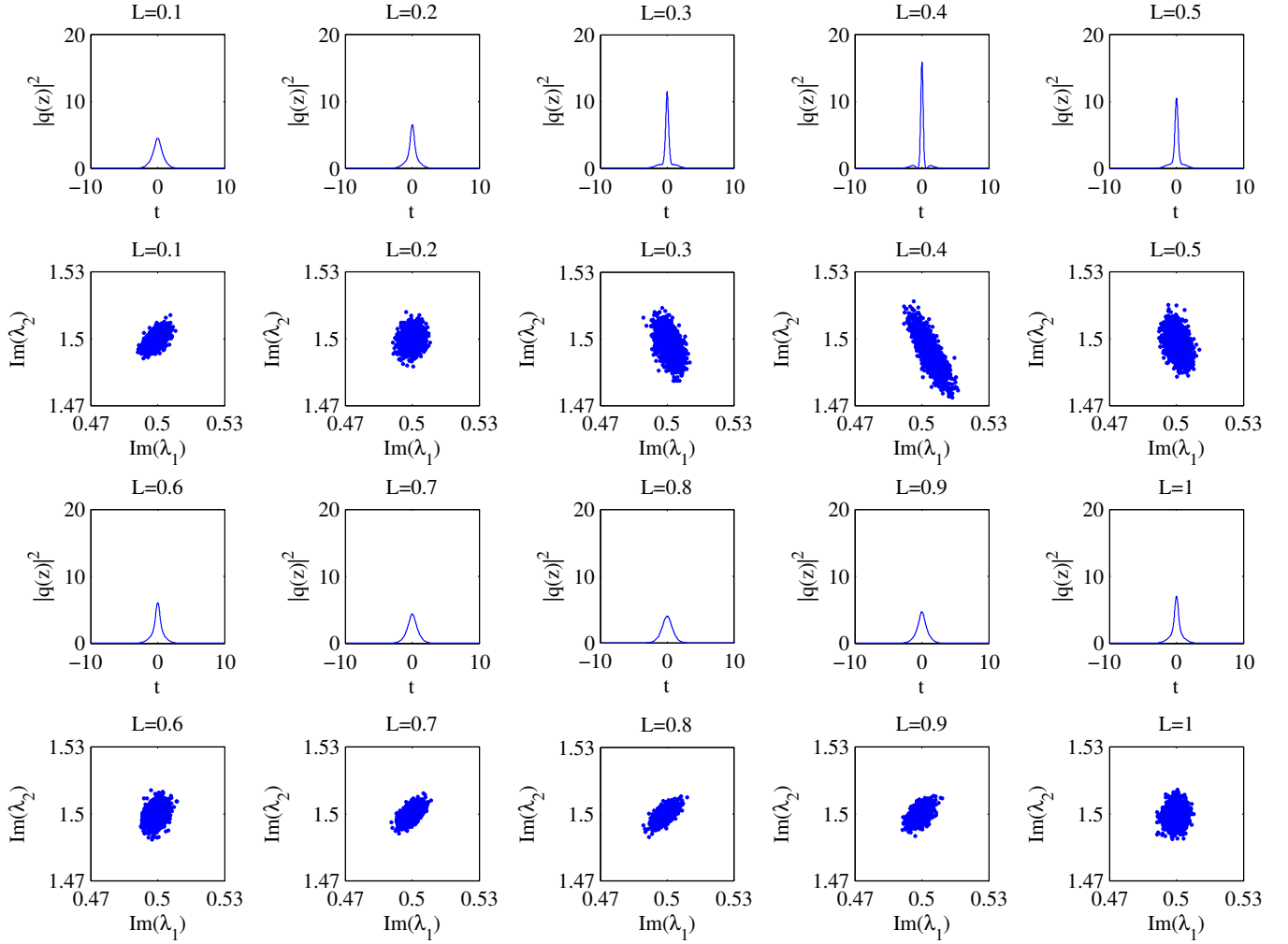


Fig. 6: Scattering plot for $\hat{\Lambda}_m$ at different normalized propagation lengths: 0.1, 0.2, 0.3, ..., 0.9, 1.0.

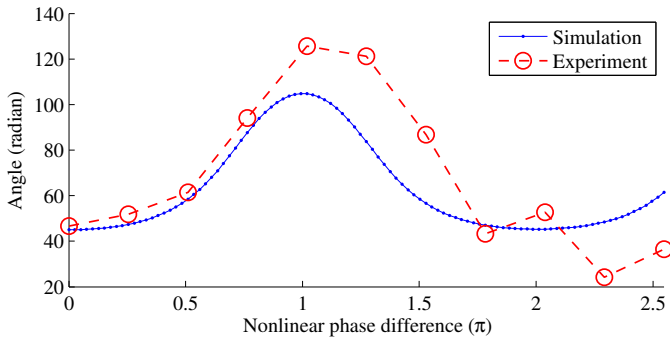


Fig. 7: NFT phase difference between Λ_1 and Λ_2

C. Simplification 2: Noise decomposition

In the previous section, we proposed a simple model to characterise the eigenvalues perturbation by modelling separately the perturbation in each individual segment. The noise added in each segment can be decomposed as the sum of many independent “noise components”. Depending on the decomposition, a noise component can be the noises added to a specific narrow frequency band or a time-interval. In our

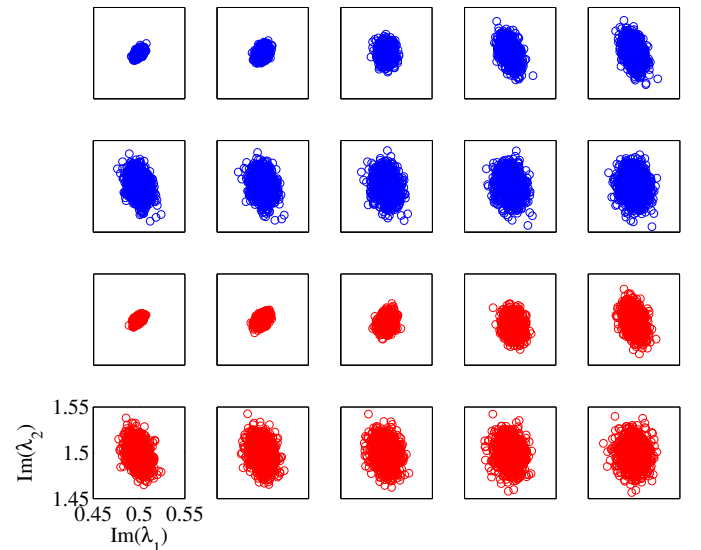


Fig. 8: Comparison of the accumulated perturbations with (top blue) and without (bottom red) the approximation Eq. (16) for m values ranging from 0.1 to 1 with a step of 0.1.

earlier work [39], we have demonstrated that noises added in frequency bands outside the signal frequency band will have minimal impacts on the perturbation of eigenvalues. In other words, in the context of detecting the eigenvalues, out of band noises are essentially irrelevant. Now, the natural question thus is: *Which “noise component” will contribute the most to the perturbation of eigenvalues?* A complete answer to the question remains unknown. In this paper, we will focus on specific noise components and investigate its contributions to eigenvalue perturbation.

We are interested in the noises of the same form as the input signal. We assume the input to the segment is $q(t)$ and $n(t)$ is the white Gaussian noise added in the segment. Define $n_1(t)$ and $n_2(t)$ such that 1) $n(t) = n_1(t) + n_2(t)$, 2) $n_1(t)$ and $n_2(t)$ are orthogonal to each other, and 3) n_1 is a scalar multiple of $q(t)$. Notice that the power of $n_1(t)$ is significantly smaller⁴ than $n_2(t)$. We will call $n_2(t)$ the residual noise and $n_1(t)$ the *scaling noise* – adding $n_1(t)$ to $q(t)$ is equivalent to multiplying $q(t)$ by a scaling factor. In the following numerical example, we will evaluate the impact of scaling noise and residual noise on discrete eigenvalues.

First, we let the signal $q(t)$ be a fundamental soliton. And we will compare the imaginary part of the discrete eigenvalues of $q(t) + n_1(t)$, $q(t) + n_2(t)$ and $q(t) + n_1(t) + n_2(t)$. Results are shown in Figure 9 and 10. In Figure 9, we consider $q(t)$ as the fundamental soliton first. The x -axis denotes the imaginary part of the discrete eigenvalue of $q(t) + n_1(t) + n_2(t)$ and the y -axis corresponds to that of $q(t) + n_1(t)$ and $q(t) + n_2(t)$. The figure clearly shows that when only $n_2(t)$ is added to the signal, the eigenvalue is largely unchanged (see the green circles data points). On the other hand, when only $n_1(t)$ is added, the eigenvalue is essentially the same as the one obtained by adding both noises together. This example illustrates that the scaling noise is dominating the perturbation of discrete eigenvalues.

Next, we consider the case when $q(t) = A \operatorname{sech}(t)$. In this case, $q(t)$ has at least two eigenvalues $A - 0.5$ and $A - 1.5$ for $A > 1.5$. In our example, we focus only on the sum of the imaginary parts of the discrete eigenvalues (which can be interpreted as the amount of energy in the solitonic component of the signal). Our simulation shows that the scaling noise n_1 has a more significant impact on the perturbation (measured by variances) of the sum of eigenvalues. Specifically, we notice that

- 1) Eigenvalue perturbations caused by addition of n_1 are often much bigger than that by addition of n_2 ;
- 2) Impact caused by n_2 on eigenvalue perturbation is at the smallest when A is close to an integer (i.e., when $q(t)$ is a multi-soliton) and is at the largest when A is slightly greater than $A - 0.5$ is slightly bigger than an integer (i.e., when $q(t)$ has an eigenvalue close to zero)
- 3) Impact caused by $n_1(t)$ is constant over regimes when $q(t)$ has the same number of discrete eigenvalues.

Motivated by our observation, we propose the following simplification: According to our previous model, eigenvalues

⁴ Strictly speaking, for white noise, $n_2(t)$ has infinite power while $n_1(t)$ has finite power.

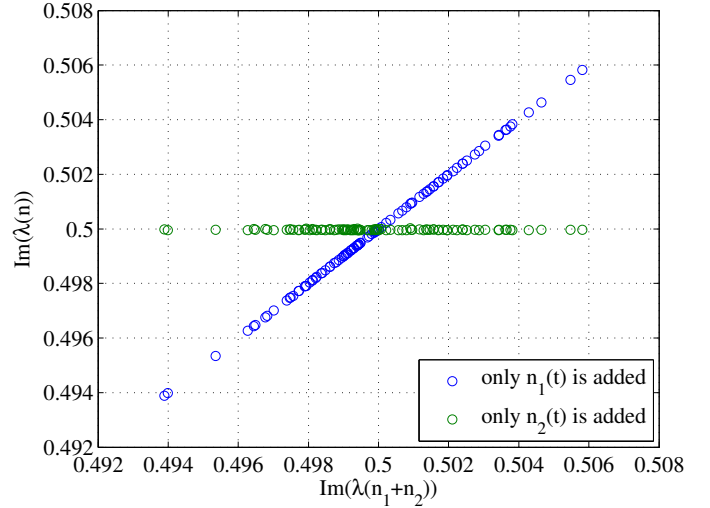


Fig. 9: Eigenvalue perturbation errors when $n_1(t)$ and $n_2(t)$ are added separately.

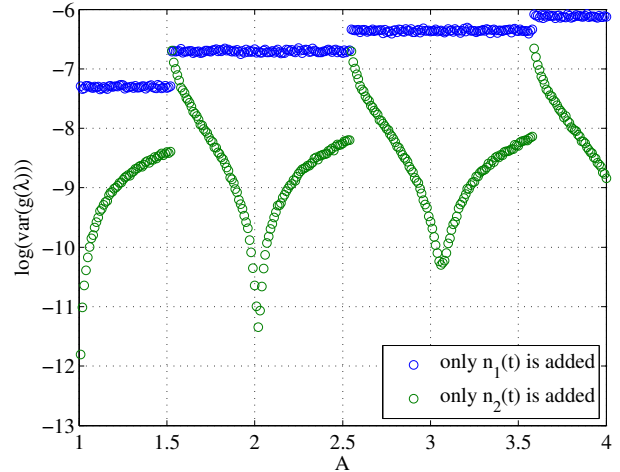


Fig. 10: Variances of eigenvalue perturbation errors when $n_1(t)$ and $n_2(t)$ are added separately

perturbation can be approximated by the sum of a collection of local perturbations $g(\hat{\Lambda}_m) - g(\Lambda_0)$ where $\hat{\Lambda}_m$ are discrete eigenvalues of $\hat{q}_m(t) \triangleq \bar{q}_m(t) + n_m(t)$.

Let $n_m^{(1)}(t)$ be the scaling noise component of $n_m(t)$,

$$\hat{q}_m(t) \triangleq \bar{q}_m(t) + n_m^{(1)}(t)$$

and $\hat{\Lambda}_m$ be its corresponding set of discrete eigenvalues. Then we can approximate $\hat{\Lambda}_m$ with $\hat{\Lambda}_m$.

Remark: The merit of the simplification is that it is analytically simpler as $n_m^{(1)}(t)$ is a one dimensional noise with finite power.

Experimental observations confirm the above claim. Consider a 2-soliton input signal with discrete eigenvalues $0.9j$ and $1.5j$. Figure 11 plots the sum of the imaginary parts of the two eigenvalues of $q_M(t)$, q^* and q^{**} as defined by; 1) $q_M(t) = q_0(t) + n_1(t) + n_2(t)$, 2) $q^*(t) = q_0(t) + n_1(t)$ and 2) $q^{**}(t) = q_0(t) + n_2(t)$. In Figure 11, the x -axis denotes

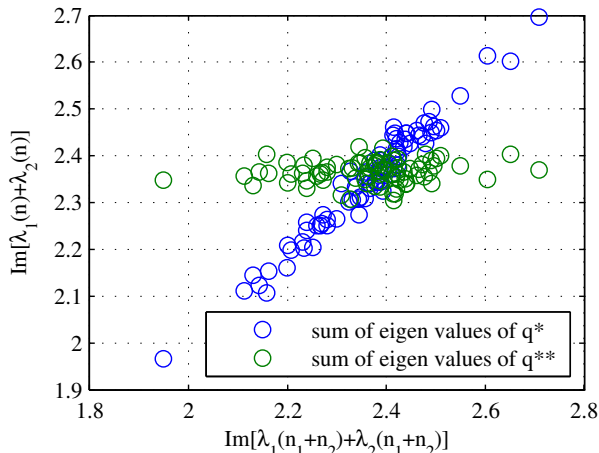


Fig. 11: Noise decomposition for 2-soliton with discrete eigenvalues $0.9j$ and $1.5j$.

the (imaginary part) of the sum of the eigenvalues of $q_M(t)$, while the y -axis denotes that of q^* and q^{**} . It is observed that the perturbation of eigenvalues of $q_M(t)$ is largely contributed by the noise $n_1(t)$.

V. Methods

A. Simulation

Numerical NFT was implemented based on the work in [6]. Forward difference method has been selected. This method recursively calculates eigenvector ν from initial condition (8). The time interval of the input signal $[T_1, T_2]$ is divided into N steps with each step size $(T_2 - T_1)/N$. The initial condition is:

$$\nu(T_1, \lambda) = \begin{pmatrix} 1 \\ 0 \end{pmatrix} e^{-j\lambda T_1}. \quad (17)$$

Once the final value i.e. eigenvector $\nu(T_2, \lambda)$ is found by recursive processing it is inserted in following equations to find $a(\lambda)$ and $b(\lambda)$:

$$a(\lambda) = \lim_{t \rightarrow \infty} \nu_1(t, \lambda) e^{j\lambda t} \quad (18)$$

$$b(\lambda) = \lim_{t \rightarrow \infty} \nu_2(t, \lambda) e^{-j\lambda t} \quad (19)$$

where $\nu(T_2, \lambda) \triangleq (\nu_1(T_2, \lambda), \nu_2(T_2, \lambda))^T$.

For the discrete spectrum, it is required to find the values of λ for which $a(\lambda)$ becomes zero. This procedure was performed by creating user defined function in MATLAB that takes initial guess value of λ and uses standard functions in MATLAB to find all λ s corresponding to $a(\lambda) = 0$. MATLAB calls that user defined function each time until it becomes zero.

The NFT code developed using the forward difference table was put to test to find eigenvalues of multiple functions e.g. fundamental soliton, non fundamental solitons, arbitrary signals and then was checked for error percentage. The error percentage was negligibly small 10^{-3} when number of steps $N > 400$. The implemented code was checked against a few typical pulses with known eigenvalues.

Numerical Nonlinear Pulse Propagation (NPP) based on split-step Fourier method has been widely used for simulations of nonlinear optical processes in wave guides. It is proven to have high accuracy in predicting pulse evolution during propagation. We used an in-house NPP software, written in C/C++, and used CUDA to parallelize the calculations by utilizing the power of graphic processing unit (GPU). This has reduced the software run-time significantly, allowing simulating a large number of instances required for statistical evaluation. In our NPP, the propagation of a pulse along a fiber is divided into length segments within which, the nonlinear and linear processes can be separated as an approximation. In each step, a band-limited white Gaussian noise is added in the frequency domain across the whole spectrum. To limit the noise bandwidth to a certain value we have used a band pass filter in the frequency domain. In order to accurately describe the statistics of the model, the same propagation simulation has been repeated for 5000 times, and eigenvalues were calculated using our numerical NFT.

B. Experiment

1) *Transmission setup*: The drive signals were converted to the analog domain by high-speed AWG (Keysight M8196A) operating at up to 92 GSa/sec. The lasers (both carrier and LO) used in the experiments external cavity lasers (ECL) emitting near 1,550 nm with a linewidth of ~ 100 kHz. The modulators used were Mach-Zehnder I/Q modulators based on LiNbO3 waveguides. A 50km Non-zero dispersion-shifted fiber (NZ-DSF) with a nonlinear Kerr coefficient $\sim 1.2W^{-1}km^{-1}$, a dispersion coefficient of $\sim 4ps \cdot nm^{-1}km^{-1}$, and 9.5 dB insertion losses was chosen as the transmission medium in the fiber loop. In this case, the distance of 150km in a normalized NLS was around 0.1, which was obtained through the variable conversion shown in [3]. Before launched into the fiber loop, the launch powers were carefully controlled by the attenuator after a fixed gain EDFA (with noise figure 5dB) to the optimum value. One extra EDFA was used to compensate for the remaining loss in the loop, and a flat-top optical filter with a 3dB bandwidth of 1nm is followed to suppress the out-of-band amplified spontaneous emission(ASE) noise. At the receiver, a polarization controller is used to align the optical signal in the x-polarization. Then the signal was detected by a dual polarization optical coherent receiver consists of a 90° hybrids and 4 balance pin-photodetector with 3dB bandwidth of ~ 38 GHz. The output 4 E-fields waveforms were sampled by a digital storage scope (Agilent 96204Q) with a sampling rate of 80GS/s and a bandwidth of 33GHz and stored to process offline.

2) *Transmitter and receiver DSP*: At the transmitter, the various 2-soliton pulses were recursively computed using the Darboux transformation method [1]. The initialization coefficients A_i and B_i for Darboux transformation method which (the discrete-spectral amplitudes and the shape of the signal) were specially choose to get smaller physical bandwidth to improve the performance at transmitter [2]. The receiver DSP firstly used a training symbol to perform timing synchronization. Then A pilot tone from y-polarization was used to

estimate and compensate the laser phase noise and frequency offsets. After normalized by a scaling factor according to the lossless path averaged model, the synchronized pulse train was processed per pulse to Search the corresponding roots. Ablowitz-Ladik algorithm was used to calculate the Nonlinear Fourier Coefficients, followed by a Newton-Raphson method for root searching [5].

VI. FURTHER WORKS AND CONCLUSIONS

This paper focuses on perturbations/noises of eigenvalues when the optical signal is transmitted along a fibre. We have numerically and experimentally demonstrated that the noises are correlated. By exploiting the correlation, one can design a better signal constellation leading to a higher system throughput. In order to take advantage of the correlation, it becomes important to derive a model of the eigenvalue noises. In the second part of the paper, we have proposed an analytical framework to characterise the noises. The idea is to decouple the eigenvalue perturbation as an accumulation of many smaller perturbations, each of which is caused by the addition of noises in a short fibre segment. As a result, one can derive an eigenvalue perturbation model by characterising each smaller perturbations. Strictly speaking, all of these small perturbations are non-identically distributed and are also correlated with each other. However, we observe that the correlation is indeed quite weak that one can essentially assume them to be independent. Following the independence relation, the perturbation in eigenvalue caused by propagation can be modeled as the accumulation of a set of independently added noise.

So far, our focus is on the eigenvalue perturbation caused by noises during signal propagation. However, our modeling framework can also be extended to included noised introduced at the transmitter and the receiver. Specifically, we will model that an additive transmitter/receiver noise will be added respectively before and after the transmission. When the transmitter and receiver noises are introduced, the signal's eigenvalues will also be perturbed. Following our paradigm, we can model the perturbations introduced at the transmitter and receiver as independent noises. Furthermore, we can also extend our work to model the perturbation of spectral amplitudes. Some preliminary correlation studies were done and can be found in [40]. In this current paper, our focus is on the perturbation of the eigenvalues. However, the same principle will also apply to spectral amplitudes as well where the overall noises in spectral amplitudes will be modeled as the accumulation of many independently distributed noises caused by the injection of noises in a short fibre segment.

REFERENCES

- [1] S. Derevyanko, J. Prilepsky, and S. Turitsyn, "Capacity estimates for optical transmission based on the nonlinear fourier transform," *Nature Communications*, 2016.
- [2] G. P. Agrawal, *Nonlinear Fiber Optics, Fifth Edition*. Springer, 2013.
- [3] R. J. Essiambre, G. Kramer, P. J. Winzer, G. J. Foschini, and B. Goebel, "Capacity limits of optical fiber networks," *J. Lightw. Technol.*, vol. 28, no. 4, pp. 662–701, Feb. 2010.
- [4] E. Ip and J. M. Kahn, "Compensation of dispersion and nonlinear impairments using digital backpropagation," *J. Lightw. Technol.*, vol. 26, no. 20, pp. 3416–3425, Oct. 2008.
- [5] A. Hasegawa and T. Nyu, "Eigenvalue communication," *J. Lightw. Technol.*, vol. 11, no. 3, pp. 395–399, Mar. 1993.
- [6] M. I. Yousefi and F. R. Kschischang, "Information transmission using the nonlinear Fourier transform, Part I: Mathematical tools," *IEEE Trans. Inf. Theory*, vol. 60, no. 7, pp. 4312–4328, Jul. 2014.
- [7] —, "Information transmission using the nonlinear fourier transform, Part II: Numerical methods," *IEEE Transactions on Information Theory*, vol. 60, no. 7, pp. 4329–4345, July 2014.
- [8] —, "Information transmission using the nonlinear fourier transform, Part III: Spectrum modulation," *IEEE Transactions on Information Theory*, vol. 60, no. 7, pp. 4346–4369, July 2014.
- [9] V. E. Zakharov and A. B. Shabat, "Exact theory of two-dimensional self-focusing and one-dimensional self-modulation of waves in nonlinear media," *Soviet Physics-JETP*, vol. 34, pp. 62–69, 1972.
- [10] M. J. Ablowitz and H. Segur, *Solitons and the Inverse Scattering Transform*. Society for Industrial and Applied Mathematics (SIAM), 2000.
- [11] M. J. Ablowitz, B. Prinari, and A. D. Trubatch, *Discrete and Continuous Nonlinear Schrödinger Systems*. Cambridge University Press, 2003.
- [12] J. Prilepsky, S. Derevyanko, K. Blow, I. Gabitov, and S. Turitsyn, "Nonlinear inverse synthesis and eigenvalue division multiplexing in optical fiber channels," *Physical Review Letters*, vol. 113, no. 1, 2014.
- [13] S. Le, J. Prilepsky, and S. Turitsyn, "Nonlinear inverse synthesis for high spectral efficiency transmission in optical fibers," *Optics Express*, vol. 22, no. 22, pp. 26 720–26 741, 2014.
- [14] S. Le, I. Philips, J. Prilepsky, P. Harper, N. Doran, A. Ellis, and S. Turitsyn, "First experimental demonstration of nonlinear inverse synthesis transmission over transoceanic distances," in *2016 Optical Fiber Communications Conference and Exhibition*, 2016.
- [15] J. Prilepsky, S. Derevyanko, and S. Turitsyn, "Nonlinear spectral management: Linearization of the lossless fiber channel," *Optics Express*, vol. 21, no. 20, pp. 24 344–24 367, 2013.
- [16] Z. Dong, S. Hari, T. Gui, K. Zhong, M. I. Yousefi, C. Lu, P. K. A. Wai, F. R. Kschischang, and A. P. T. Lau, "Nonlinear Frequency Division Multiplexed Transmissions Based on NFT," *IEEE Photonics Technology Letters*, vol. 27, no. 15, pp. 1621–1623, Aug. 2015.
- [17] H. Terauchi and A. Maruta, "Eigenvalue modulated optical transmission system based on digital coherent technology," *18th OptoElectronics and Communications Conference Held Jointly with 2013 International Conference on Photonics in Switching*, 2013.
- [18] A. Maruta, "Eigenvalue modulated optical transmission system," *Proceedings of the 20th OptoElectronics and Communications Conference (OECC)*, 2015.
- [19] E. Meron, M. Shtaif, and M. Feder, "Beneficial use of spectral broadening resulting from the nonlinearity of the fiber-optic channel," *Optics Letters*, vol. 37, no. 21, pp. 4458–4460, 2012.
- [20] S.-I. Oda, A. Maruta, and K.-I. Kitayama, "All-optical quantization scheme based on fiber nonlinearity," *IEEE Photonics Technology Letters*, vol. 16, no. 2, pp. 587–589, 2004.
- [21] H. Bulow, "Experimental demonstration of optical signal detection using nonlinear fourier transform," *Journal of Lightwave Technology*, vol. 33, no. 7, pp. 1433–1439, 2015.
- [22] V. Aref, H. Bulow, K. Schuh, and W. Idler, "Experimental demonstration of nonlinear frequency division multiplexed transmission," in *European Conference on Optical Communication, ECOC*, vol. 2015–November, 2015.
- [23] T. H. Zhang, Qun; Chan, "On the model consistency of soliton communication systems," in *IEEE 16th International Workshop on Signal Processing Advances in Wireless Communications (Stockholm, Sweden)*, 2015.
- [24] S. Derevyanko, J. Prilepsky, and S. Turitsyn, "Capacity estimates for optical transmission based on the nonlinear fourier transform," *Nature Communications*, vol. 7, 2016.
- [25] C. W. Gardiner and P. Zoller, *Quantum Noise: A Handbook of Markovian and Non-Markovian Quantum Stochastic Methods With Applications to Quantum Optics, Third Edition*. Springer-Verlag, New York, 2004.
- [26] A. Mecozzi, "Limits to long-haul coherent transmission set by the Kerr nonlinearity and noise of the in-line amplifiers," *J. Lightw. Technol.*, vol. 12, no. 11, pp. 1993–2000, Nov. 1994.
- [27] E. Iannone, F. Matera, A. Mecozzi, and M. Settembre, *Nonlinear Optical Communication Networks*. Wiley, New York, 1998.
- [28] L. F. Mollenauer and J. P. Gordon, *Solitons in Optical Fibers: Fundamentals and Applications*. Academic Press, San Diego, 2006.
- [29] J. P. Gordon and H. A. Haus, "Random walk of coherently amplified solitons in optical fiber transmission," *Opt. Lett.*, vol. 11, no. 10, pp. 665–667, Oct. 1986.

- [30] A. Mecozzi, J. D. Moores, H. A. Haus, and Y. Lai, "Soliton transmission control," *Opt. Lett.*, vol. 16, no. 23, pp. 1841–1843, 1991.
- [31] L. F. Mollenauer, J. P. Gordon, and S. G. Evangelides, "The sliding-frequency guiding filter: an improved form of soliton jitter control," *Opt. Lett.*, vol. 17, no. 22, pp. 1575–1577, 1992.
- [32] M. Nakazawa, K. Yamada, H. Kubota, and E. Suzuki, "10 Gbit/s soliton data transmission over one million kilometres," *Electron. Lett.*, vol. 14, no. 27, pp. 1270–1272, Jul. 1991.
- [33] A. Mecozzi, "Soliton transmission control by Butterworth filters," *Opt. Lett.*, vol. 20, no. 18, pp. 1859–1860, 1995.
- [34] J. P. Gordon and L. F. Mollenauer, "Phase noise in photonic communications systems using linear amplifiers," *Opt. Lett.*, vol. 15, no. 23, pp. 1351–1353, 1990.
- [35] M. Hanna, H. Porte, J. P. Goedgebuer, and W. T. Rhodes, "Soliton optical phase control by use of in-line filters," *Opt. Lett.*, vol. 24, no. 11, pp. 732–734, 1999.
- [36] —, "Experimental investigation of soliton optical phase jitter," *IEEE J. Quantum Electron.*, vol. 36, no. 11, pp. 1333–1338, Nov. 2000.
- [37] —, "Performance assesment of DPSK soliton transmission system," *Electron. Lett.*, vol. 37, no. 10, pp. 644–646, May 2001.
- [38] C. J. McKinstrie and C. Xie, "Phase jitter in single-channel soliton systems with constant dispersion," *IEEE J. Sel. Topics Quantum Electron.*, vol. 8, no. 3, pp. 616–625, Aug. 2002.
- [39] K. Amir, W. Q. Zhang, Q. Zhang, T. H. Chan, and S. Afshar V, "Noise effect on the nonlinear fourier transform," in *Australian and New Zealand Conference on Optics and Photonics*, 2015.
- [40] T. Gui, T. H. Chan, C. Lu, A. P. T. Lau, and P. K. A. Wai, "Alternative Decoding Methods for Optical Communications Based on Nonlinear Fourier Transform," *Journal of Lightwave Technology*, vol. 35, no. 9, pp. 1542–1550, May 2017.

APPENDIX A SUPPLEMENTARY MATERIALS

A. Effect of different noise on eigenvalue distribution

In order to investigate collectively the effects of noise at different stages of pulse generation, we consider the most general form of noise (which can be various kinds of amplitude, phase and background noise) as follows:

$$[A_0 + A(t)] q(t) e^{2\pi i * i * [B_0 + B(t)]} + C_0 + C(t), \quad (20)$$

where $A_0, A(t), C_0, C(t)$ are complex, and B_0 and $B(t)$ are real. We study the effect of different types of noise by allowing noise in each of $A_0, A(t), C_0, C(t), B_0$ and $B(t)$ separately. The following figures (12) show the NFT eigenvalue distributions for the 2-eigenvalue pulses (the same eigenvalue sets as the system described in Fig. 2 in the main document) when noise is added to each of the coefficients individually. All figures, except Fig. 12(e), represent similar trend; positive correlation and elliptical shape distribution with minor and major axes whose values and orientations⁵ depend on the values of the set of $(\lambda_1$ and $\lambda_2)$. It is also observed that comparatively constant noises have less impact on the orientation, values of minor and major axes, and shifting of the mean values of each set than those of time-varying noises. Among time-varying noises, the phase noise, Fig. (12f) has the most impact in terms of shifting the mean values of each set. Note that constant phase noise, on the contrary, has no effect on the distribution of eigenvalues whatsoever. This agrees with analysis where it is well known that constant phase changes have no impact on discrete eigenvalues (but only on the corresponding spectral

⁵ For each group of simulation/experiment, a set of 2-dimensional data points (whose coordinates are the discrete eigenvalues of the received signals) will be generated. These data points further defines an empirical covariance matrix. Its orientation is defined as the slope of the principal eigenvector of the covariance matrix.

amplitudes). Although the exact contribution each type of the noise is unknown, the difference between the experimental observation and simulation can attributed to these types of noise.

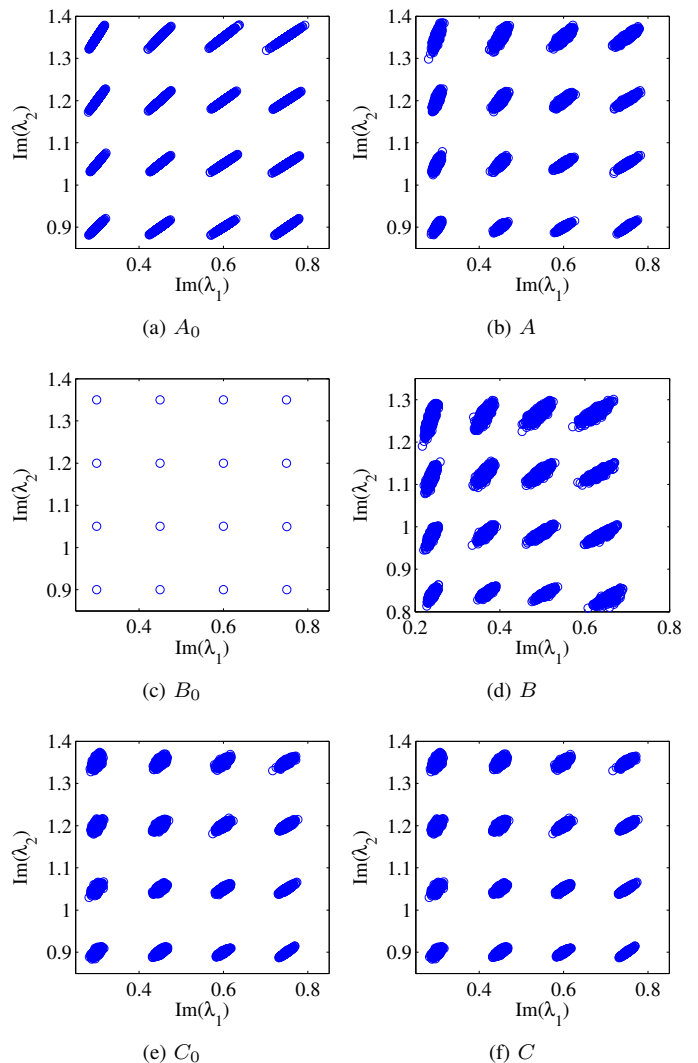


Fig. 12: The effect of different types of noises on NFT eigenvalues.

B. Channel noise modeling via linearisation

In this paper, we proposed a method to model perturbation eigenvalues. As an analogy, our approach is in fact similar to the idea of approximating a nonlinear function with a piecewise linear function via the approximation that

$$\begin{aligned} f(x_o + \delta_1 + \delta_2) - f(x_o) \\ \approx f(x_o + \delta_1) - f(x_o) + f(x_o + \delta_2) - f(x_o) \end{aligned} \quad (21)$$

In other words, the error in the function f caused by the noises δ_1 and δ_2 (either added simultaneously or sequentially) is roughly equal to the sum of errors induced by δ_1 and δ_2 separately. In the following, we will further elaborate our results in details.

Our first step is to verify if similar “linearity” in (21) also holds or not in our application. Consider the following simple scenario. Let $q_0(t)$ be an input signal and $\Lambda_0 = (\lambda_{0,i}, i \in |\Lambda_0|)$ be its corresponding set of discrete eigenvalues and $g(\Lambda_0)$ be a function of Λ_0 of interest. Note that $g(\cdot)$ can be a vector-valued function in general. The following are some examples:

$$g(\Lambda_0) \triangleq \min_{i=1,\dots,|\Lambda_0|} \text{imag}(\lambda_{0,i}), \quad (22)$$

$$g(\Lambda_0) \triangleq \max_{i=1,\dots,|\Lambda_0|} \text{imag}(\lambda_{0,i}), \quad (23)$$

or

$$g(\lambda_0) \triangleq \sum_{i=1,\dots,|\Lambda_0|} \text{imag}(\lambda_{0,i}). \quad (24)$$

Now, consider two noises $n_1(t)$ and $n_2(t)$. Let

$$q_1(t) = q_0(t) + n_1(t)$$

$$q_2(t) = q_0(t) + n_2(t)$$

$$q_3(t) = q_0(t) + n_1(t) + n_2(t).$$

The addition of noises will cause the discrete eigenvalue to perturb. Specifically, let $\Lambda_k = (\lambda_{k,i}, i \in |\Lambda_k|)$ be the eigenvalues of q_k respectively for $k = 1, 2, 3$. Now, the question is to determine whether

$$g(\Lambda_3) - g(\Lambda_0) \approx g(\Lambda_1) - g(\Lambda_0) + g(\Lambda_2) - g(\Lambda_0) \quad (25)$$

holds or not.

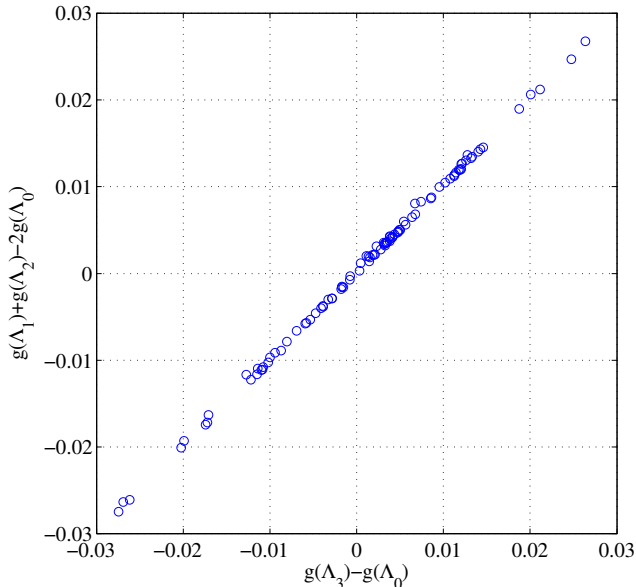


Fig. 13: Eigenvalue perturbations add up linearly.

To answer the question, we conduct the following numerical example, in which two Gaussian noises ($n_1(t)$ and $n_2(t)$) are added to a 2-soliton $q_0(t)$. We consider a scalar-valued function g as defined in (24), which can be interpreted as the energy of the signal’s solitonic components. Results are shown in Figure 13 where the x -axis corresponds to $g(\Lambda_3) - g(\Lambda_0)$ and the

y -axis corresponds to $g(\Lambda_1) + g(\Lambda_2) - 2g(\Lambda_0)$. Our numerical example clearly indicates that the two quantities are basically the same suggesting that “linearity” in (25) does hold. The previous example suggests that the errors/perturbations on the eigenvalues are in fact linear – that the accumulated errors induced by the addition of two noises is approximately the sum of the two errors induced by the noises separately. Next, we will consider the case when the noises are added in a distributed manner along the fibre.

C. Transmitter and propagation noise

In section IV B, an experiment was conducted to demonstrate that perturbation of discrete eigenvalues caused by addition of point noise is input dependent (or more precisely, depends on the NFT phase of the pulse in that example). In the experiment, transmitter noise was not considered effecting the outcome and the propagation noise in the fiber is less significant than the receiver noise. To support this assumption, Fig.14 and Fig.15 are produced. Fig.14 is a numerical simulation of a collection of pulses with noise added prior to a noiseless propagation for a distance corresponding to π NFT phase (maximum change in the orientation of the covariance matrix). The results indicate the covariance matrix of the pulses after propagation (red circles) is the same as the pulses before propagation (blue dots). In other words, the noise generated in the transmitter does not effect the experiment.

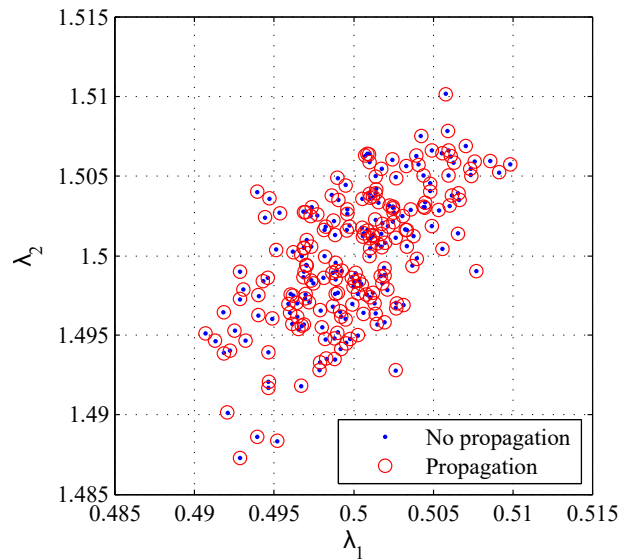


Fig. 14: Eigenvalue perturbations caused by transmitter noise.

Fig. 15 shows the comparison of the covariance matrix of the experimental data sets for 0 km and 150 km of fiber propagation respectively. The variances along the primary axis are $2.48e-3$ for 0 km and $2.28e-3$ for 150 km. The covariances are $1.16e-3$ for 0 km and $1.01e-3$ for 150 km. We consider this amount of change in the variances to be small and thus noise added during the propagation through fiber is small comparing to the noise in the transmitter and the receiver.

In summary, the transmitter noise does not contribute to the changes of the covariance matrix of the received signals.

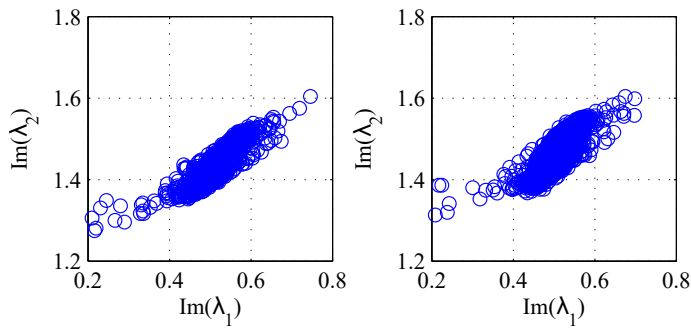


Fig. 15: Eigenvalue perturbations in experiment. (Left) Back to back pulses. (Right) Pulses after 150 km propagation.

The noise added to the signals during propagation is relatively small. Therefore, the observed rotation of the primary axis of the covariance matrix at different propagation length is mainly due to the noises added at the receiver. Hence, the experiment is equivalent to a point noise added to pulses with different NFT phases.

To see this, first, all the transmitter noise added at the input of the fibre are the same (as they all have the same input pulses). Second, as eigenvalues are invariant under the noiseless propagation, the perturbation of eigenvalues we see at the end of the fibre caused by the transmitter noise will be also be the same as the input. In other words, the noise at the output due to the transmitting stage will be the same for all experiment.